Journal of Molecular Spectroscopy 395 (2023) 111797

Contents lists available at ScienceDirect

Journal of Molecular Spectroscopy

journal homepage: www.elsevier.com/locate/yjmsp

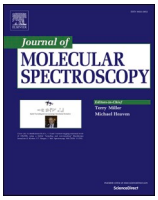

The ground, $v_2 = 1$, 2 and $v_4 = 1$ states of $^{14}ND_3$ analyzed at experimental accuracy

Elisabetta Canè [a,*], Gianfranco Di Lonardo [a], Luciano Fusina [a], Adriana Predoi-Cross [b], Filippo Tamassia [a]

[a] Dipartimento di Chimica Industriale "Toso Montanari", Università di Bologna, Viale Risorgimento 4, 40136 Bologna, Italy
[b] Faculty of Science and Technology, Athabasca University, 1 University Drive, Athabasca T9S 3A3, Canada

ARTICLE INFO

Keywords:
Per-deuterated ammonia
ND_3
High resolution infrared spectra
Ground state parameters
Ro-vibration analysis
Bending states analysis

ABSTRACT

Ammonia is the object of extensive investigations due to the peculiar pattern of its interacting vibration states and its central role in astronomical sciences. $^{14}ND_3$ is of interest in astrochemistry because the determination of deuterium fractionation ratios in ammonia and its deuterated isotopologues contributes to a deeper knowledge of the chemistry in the cold, dense cores of the interstellar medium. Here, the ground, $v_2 = 1$, 2 and $v_4 = 1$, *a*, *s* states of $^{14}ND_3$ are analyzed thanks to new spectra recorded with the Canadian Light Source synchrotron, from 60 to 1500 cm^{-1} at a resolution ranging from 0.00096 to 0.003 cm^{-1}. Overall, 7765 inversion, rotation-inversion, and vibration–rotation-inversion transitions in ν_2, $2\nu_2$, ν_4, $2\nu_2 \leftarrow \nu_2$, $2\nu_2 \leftarrow \nu_4$, $\nu_4 \leftarrow \nu_2$, $\nu_2 \leftarrow \nu_2$, $2\nu_2 \leftarrow 2\nu_2$, and $\nu_4 \leftarrow \nu_4$ have been fitted simultaneously to characterize the *s* and *a* levels of the excited states. 4021 and 2388 transitions were assigned in the cold and hot bands, respectively, and 150 inversion and 1206 inversion-rotation transitions in $v_2 = 1$, 2 and $v_4 = 1$. The effective Hamiltonian adopted includes all symmetry allowed interactions between and within the studied excited states, according to the most recent results on ammonia. The transitions have been reproduced at experimental accuracy using 118 spectroscopic parameters, determined with high precision. In addition, a new analysis of the ground state has been performed. 9256 data have been fitted, 78 inversion and 837 rotation-inversion transitions, and 8341 ground state combination differences. An improved set of parameters and term values are derived thanks to the increased precision of the newly assigned rotation-inversion transitions with *J*/ *K* values up to 31/30 and to the larger number of the ground state combination differences.

1. Introduction

The scientific investigations on ammonia are continuously prompted forward by its prominent role in fundamental and applied high resolution molecular spectroscopy [1–4]. Reliable and extensive spectroscopic datasets are essential to monitor this molecule in Earth's [5], planetary [6] and exoplanet atmospheres [7], to probe the physical conditions in dense molecular cold cores through ammonia depletion [8] and to understand the astrochemistry of stellar systems [9]. The perdeuterated isotopologue of ammonia, $^{14}ND_3$, became of astrophysical interest since its first detection in very young protostars [10] and in the cold, dense interstellar medium [11] prior to star formation. Its discovery has contributed to a significant revision of low temperature ion–molecule chemistry. In particular, the amount of deuterium fractionation in ammonia has been used as a powerful probe to trace the evolutionary stage of dense cores from both physical and chemical points of view [12–16].

$^{14}ND_3$ has been the object of spectroscopic studies in the microwave (MW), millimeter-wave (mmW) and infrared (IR) regions, as recently reported by Canè at al. in Ref. [17]. The ro-vibration analyses of the fundamentals, previously based on the dyad approach [18,19], were improved including the first overtones of the bending vibrations with close energies, $2\nu_2$ and $2\nu_4$. A comprehensive treatment of 3436 and 2408 transitions of the $\nu_2/\nu_4/2\nu_2$ and $\nu_1/\nu_3/2\nu_4$ vibration systems, respectively, was successfully achieved. The adopted effective Hamiltonian included all symmetry allowed interactions between and within the excited state levels in each band system and precise spectroscopic parameters were obtained for both inversion components of the studied vibration states [17]. Next, the perturbation allowed transitions identified in the ν_1, ν_2, ν_3, ν_4, and $2\nu_4$ bands were combined to the allowed

* Corresponding author at: Dipartimento di Chimica Industriale "Toso Montanari", Viale del Risorgimento 4, 40136 Bologna, Italy.
E-mail address: elisabetta.cane@unibo.it (E. Canè).

https://doi.org/10.1016/j.jms.2023.111797
Received 20 April 2023; Received in revised form 1 June 2023; Accepted 3 June 2023
Available online 7 June 2023
0022-2852/© 2023 The Authors. Published by Elsevier Inc. This is an open access article under the CC BY license (http://creativecommons.org/licenses/by/4.0/).

transitions to obtain ground state combination differences (GSCD) connecting levels of the ground state (GS) with different K values. They allowed the determination from experiment, for the first time, of precise K-dependent constants ${}^{(a,s)}C$, ${}^{(a,s)}D_K$, and ${}^{(a,s)}H_K$ in the GS of $^{14}ND_3$ [20]. The improved characterization of the GS prompted us to further investigate the vibrationally excited states recording new Fourier transform infrared (FTIR) spectra of $^{14}ND_3$ at the Canadian Light Source, CLS, in Saskatoon, Canada, by means of the synchrotron radiation. The aim was to improve the knowledge of the ground and of the $v_2 = 1$, 2 and $v_4 = 1$ a, s inversion levels exploiting the enhanced instrumental sensitivity, spectral resolution and wavenumber precision.

Here the analyses of the new spectra from 60 up to about 1500 cm^{-1} of $^{14}ND_3$ are presented. The assignment of vibration -rotation-inversion transitions in ν_2, ν_4, and $2\nu_2$ and in the $2\nu_2 \leftarrow \nu_2$ hot band were extended at higher J, K values. In addition, transitions in the $\nu_4 \leftarrow \nu_2$ and in the weaker $2\nu_2 \leftarrow \nu_4$ hot bands were assigned for the first time. In the far infrared (FIR) region of the spectra rotation-inversion transitions have been identified in the GS up to high J and K values and assigned in the $v_2 = 1$, 2 and $v_4 = 1$ a, s inversion state levels for the first time. Moreover, all the transitions previously reported [17,20] have been re-measured with higher experimental precision. In total, 7765 transitions comprising those in the bands ν_2, $2\nu_2$, ν_4, $2\nu_2 \leftarrow \nu_2$, $2\nu_2 \leftarrow \nu_4$ and $\nu_4 \leftarrow \nu_2$, and the inversion-rotation transitions in the $v_2 = 1$, 2, and $v_4 = 1$ excited states (see in Fig. 1 the type of transitions connecting the states observed in this study) have been fitted simultaneously. The effective Hamiltonian adopted includes all symmetry allowed interactions between and within the studied excited states, according to our most recent results on $^{15}NH_3$ [21]. The transitions have been reproduced at experimental accuracy using 118 spectroscopic parameters, determined with high precision.

Rotation-inversion transitions in the GS have been extended up to J' and $K' = 31$, 30 and analyzed together with the GSCD calculated from 3696 transitions presently measured in ν_2, ν_4, and $2\nu_2$ infrared bands and from those in ν_1, ν_3, and $2\nu_4$, 4645 data [20]. An improved and extended set of GS parameters and term values are obtained.

The paper is structured as follows: the experimental details are given in Section 2; the description of the spectra and the procedure adopted for the assignments are given in Section 3; the theoretical model and the results of the fits are described in Section 4 while the conclusions are drawn in Section 5.

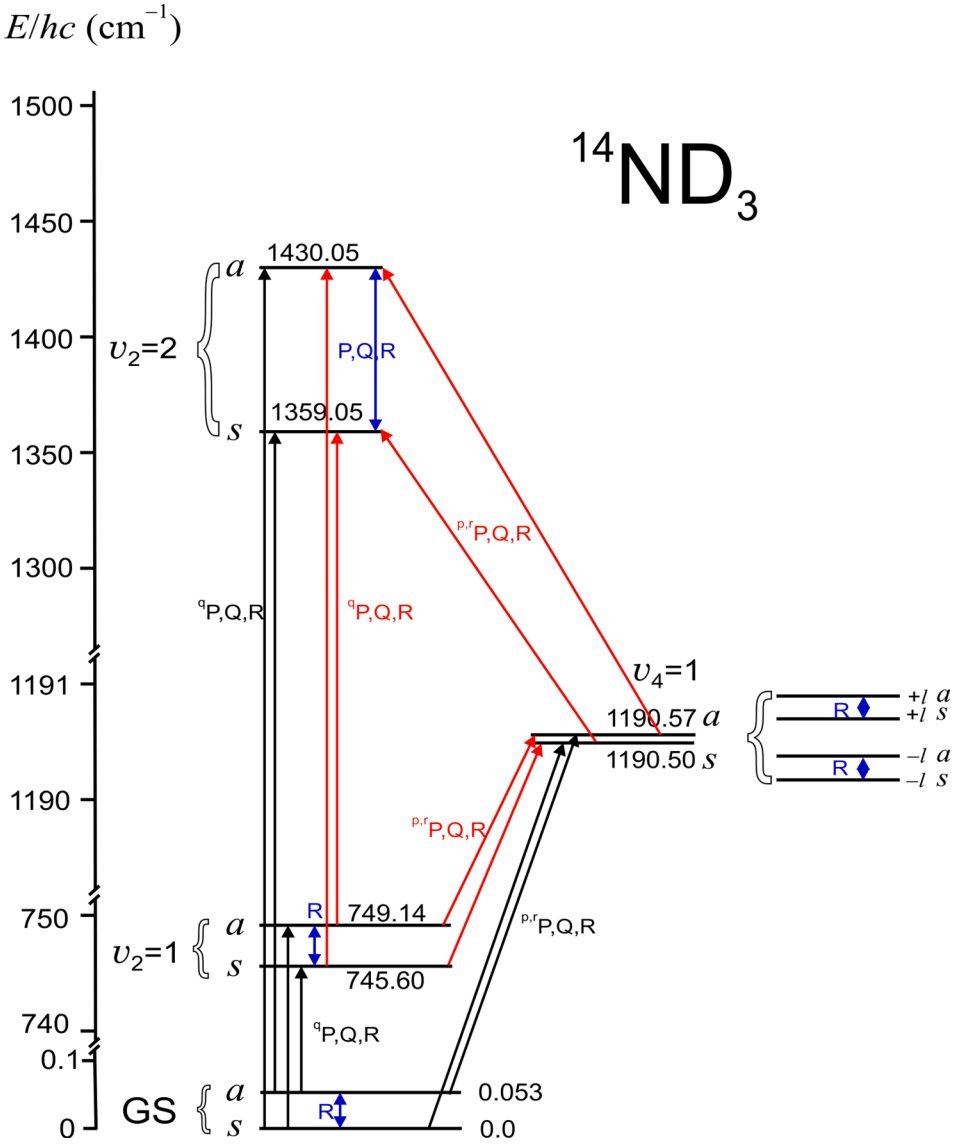

Fig. 1. Energy diagram of $^{14}ND_3$ showing the GS and the excited vibration states up to 1500 cm^{-1}. Observed experimental term values are given in cm^{-1}. The vibration–rotation-inversion transitions are indicated by black and red arrows, for the cold and hot bands, respectively. The rotation-inversion and pure inversion transitions are indicated by blue arrows. (For interpretation of the references to colour in this figure legend, the reader is referred to the web version of this article.)

2. Experimental details

Eight spectra were recorded using the Bruker IFS 125 FT spectrometer located at the FIR beam line, CLS [22]. All spectra were obtained at room temperature using two identical samples of $^{14}ND_3$ supplied by Sigma-Aldrich with a stated isotopic purity of 99%. The recorded spectra showed a sample composition of about 60% of ND_3, 30% of ND_2H, 10% of NH_2D, and traces of NH_3, H_2O, and HOD. The experimental conditions for the spectral recordings are given in Table 1. The spectra 1 to 4 were recorded in the region between 60 and 610 cm^{-1} at 0.00096 cm^{-1} unapodized instrumental resolution. Optimum instrumental performance was achieved using the synchrotron radiation, 6 μm mylar beam splitter and a Si bolometer cooled at 4 K. The spectrometer aperture was set to 1.5 mm. Spectra 5 to 8 were recorded using the synchrotron light, a KBr beam splitter, and two different detectors. A Cu doped Ge detector was used for spectra 5 to 7 while for spectrum 8 a HgCdTe detector was adopted; they were cooled at 4 K and 77 K, respectively. A scanner velocity of 80 kHz was used with analog electronic filter set for a low band pass of 5 kHz. No optical filter was used. Before applying apodization, during the Fourier transform the instrumental line width was 0.00096 cm^{-1}, measured full width half maximum. Zero-filling factor of 2, Mertz phase correction, and phase resolution of 1.0 were also used in the Fourier transformation of the interferograms.

The spectra were recorded using a temperature controlled multi pass absorption cell (White cell) with 2 m base. The gas pressure was measured using a 0–1 Torr Baratron gauge. Water lines [23] were used to calibrate the wavenumber scale. The impurities identified in the spectra were $^{14}NH_3$, H_2O and HOD. The estimated wavenumber uncertainty of isolated lines of medium intensity is 0.1–0.4 × 10^{-3} cm^{-1} depending on their position in the spectrum and on the sample pressure.

3. Assignments and description of the spectra

The spectra are crowded for the presence of the absorption lines from all ^{14}N deuterated isotopologues of ammonia: ND_3, ND_2H, and NH_2D. Due to their relative proportion, 60, 30, and 10 %, respectively, we recently used these spectra to re-analyze the GS of the partially deuterated species [24]. For ND_3, the inspection of the IR spectra was first devoted to identify vibration-rotation-inversion transitions in ν_2, ν_4, $2\nu_2$, unassigned in [17]. In fact, the enhanced sensitivity and resolution of the present spectral recordings allow the observation of very weak absorptions, corresponding to transitions with high J and K values or perturbation allowed ones. To assist the new assignments the wavenumbers of the predicted transitions were calculated using the spectroscopic parameters of the ground and of the excited states from [17,20] and the model Hamiltonian in [21]. After the completion of the assignments, all vibration-rotation-inversion transitions were fitted simultaneously to refine the spectroscopic parameters in the $v_2 = 1$, 2 and $v_4 = 1$ a, s states (see below). Those parameters were used to calculate new term values of the a, s excited state levels to predict the wavenumber transitions of the $2\nu_2 \leftarrow \nu_2$, $\nu_4 \leftarrow \nu_2$ and the weaker $2\nu_2 \leftarrow \nu_4$ hot bands and of the inversion and rotation-inversion transitions. Their search in the FIR and IR regions resulted greatly facilitated by the precision of their calculated values. As a result, all wavenumbers of the $2\nu_2 \leftarrow \nu_2$ transitions in [17] were measured at higher precision, 0.4 × 10^{-3} cm^{-1} instead of 0.6 × 10^{-3} cm^{-1}, and the assignments have been extended from $J', K' = 18,18$ to 19,19 ($s \leftarrow a$) and from 17,17 to 19,18 ($a \leftarrow s$), respectively. The $\nu_4 \leftarrow \nu_2$ and $2\nu_2 \leftarrow \nu_4$ transitions, ($a \leftarrow a$), ($s \leftarrow s$), have been identified for the first time up to J', $K' = 17,17$ and 12,10, respectively. The assignment procedure was accomplished in an iterative process, which consists of improving the values of the spectroscopic parameters by means of the newly assigned lines, predicting the wavenumbers of higher J and K transitions to be searched in the spectra, enlarging the data set, and so on, until all the transitions that could be unambiguously assigned were identified. The new assignments have been also checked by means of the precise GSCD or of the lower state combination differences (LSCD), for the hot bands. Finally, about two hundred and fifty perturbation allowed transitions, according to the $\Delta J = 0, \pm 1, \Delta(k - l) = \pm 3$ selection rules, have been identified in ν_4 and to a minor extent in ν_2.

Some pictures of the rotation-inversion absorptions in the GS and in the $v_2 = 1$ and $v_4 = 1$ states are shown in Figs. 2-4 while an example of the $2\nu_2 \leftarrow \nu_2$ hot band transitions is illustrated in Fig. 3 of Ref. [17].

In Fig. 2 the $R_K(9)$, $\Delta J = +1$, $\Delta K = 0$ $s \leftarrow a$ and $a \leftarrow s$ transitions in the GS are shown. Their K structures are blue degraded and intermingled owing to the small value of inversion splitting, 0.053 cm^{-1}. The 1 to 10 ratio of the spin statistical weight of the $K = 0$, s and a components of the inversion doublet, for odd J value, is apparent in the relative intensity of the corresponding transition lines. Only one strong absorption is observed for $K = 3$ instead of the expected doublet, with relative intensity 10:1, since both components of the $K = 3$ doublets are resolved for only $J'' > 9$. An explicative energy diagram for the GS and non-degenerate excited states of ND_3 for $K = 0$ and 3, with the different types of weak or strong transitions connecting the levels is depicted in Fig. 5.

In Fig. 3 the $R_K(12)$ $s \leftarrow a$ rotation-inversion transitions in $v_2 = 1$ are shown, with the $K = 0$, and $K = 1$ lines overlapped. Only the $s \leftarrow a$ transitions are present in the illustrated spectral interval owing to the larger a, s energy separation in $v_2 = 1$, 3.54 cm^{-1}, with respect to the GS. The corresponding $a \leftarrow s$ transitions are observed between 133.61 and 136.76 cm^{-1}. Differently from Fig. 2 the K structure is red degraded for increasing K. The complicated spectral features of the $s \leftarrow a$ and $a \leftarrow s$, $\Delta J = +1$ and $\Delta K = 0$ rotation-inversion transitions for $J'' = 10$ in $v_4 = 1$, $l = -1$, are shown in Fig. 4. They are quite intermingled since the a, s energy separation is 0.07 cm^{-1}. Being $v_4 = 1$ doubly degenerate, two sets of levels, corresponding to the vibration angular momentum $l = \pm 1$, are present for each inversion state. Four branches are observed in the spectrum for each $J + 1 \leftarrow J$ transition because the selection rules for rotation-inversion transitions are: $\Delta l = 0$, $\Delta J = \pm 1$, $\Delta K = 0$, $a \leftarrow s$ and $s \leftarrow a$. In Fig. 4 both branches are red degrading for increasing K but invert their direction for high K values. The splitting of the $K = 2$ levels is evident in both series.

Once the assignment procedure was completed, 4020 transitions in ν_2, ν_4, and $2\nu_2$, 2388 transitions in the hot bands, 150 inversion and 1207 rotation-inversion transitions in $v_2 = 1$, 2 and $v_4 = 1$, presently measured or reported in the literature, have been analyzed simultaneously. The final dataset for the analysis of the excited states contains 7765 transitions distributed among the analyzed bands as listed in Table 2, where the number and characteristics of each subset are specified.

A single wavenumber for each assigned transition has been considered, choosing the one with the lowest uncertainty in case of alternative measurements. The types of observed transitions are drawn as arrows with different colors in the scheme of the energy states of $^{14}ND_3$ in Fig. 1.

The final database for the GS analysis contains 9256 data: 78 inversion, 837 rotation-inversion transitions and 8341 GSCD, 3696 from transitions in ν_2, $2\nu_2$, and ν_4 bands and 4645 from ν_1, $2\nu_4$, ν_3 [20]. The number and characteristics of each subset are specified in Table 3.

Table 1
Experimental conditions of the FTIR spectra of $^{14}ND_3$ recorded at 297 K.

no.	spectral region /cm^{-1}	sample pressure/Pa	path length/m	instrumental resolution/cm^{-1}
1	60–610	1.33	72	0.00096
2	60–610	6.67	8	0.00096
3	60–610	13.33	72	0.00096
4	60–610	133.32	72	0.00096
5	425–1250	13.33	72	0.003
6	425–1250	133.32	72	0.003
7	500–1250	0.13	72	0.003
8	700–1515	133.32	72	0.003

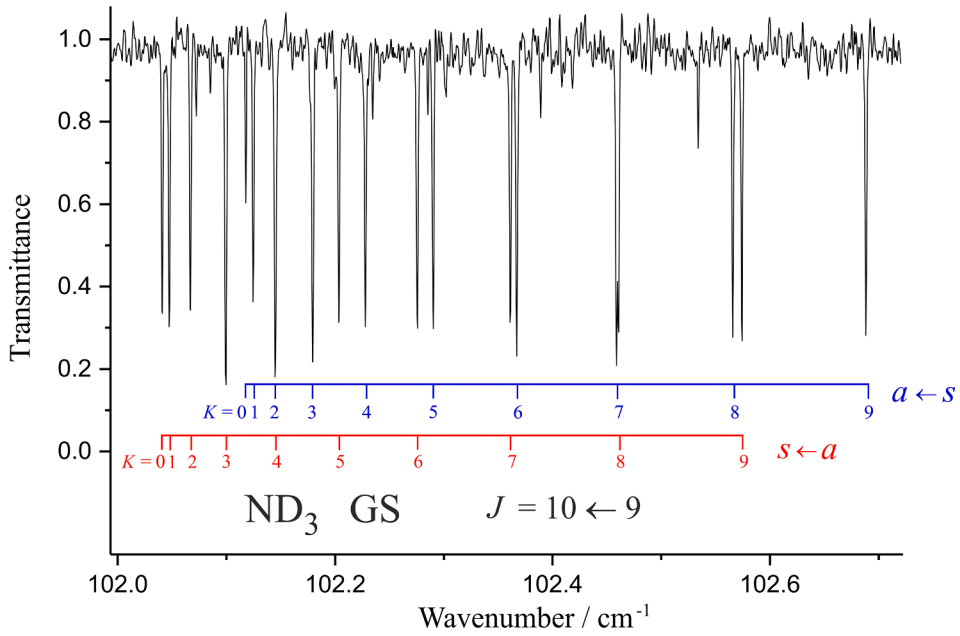

Fig. 2. Portion of the GS rotation-inversion spectrum for ND_3 showing the $s \leftarrow a$ and $a \leftarrow s$ $R_K(9)$ transitions. Experiment: see the recording conditions of spectrum 1 in Table 1.

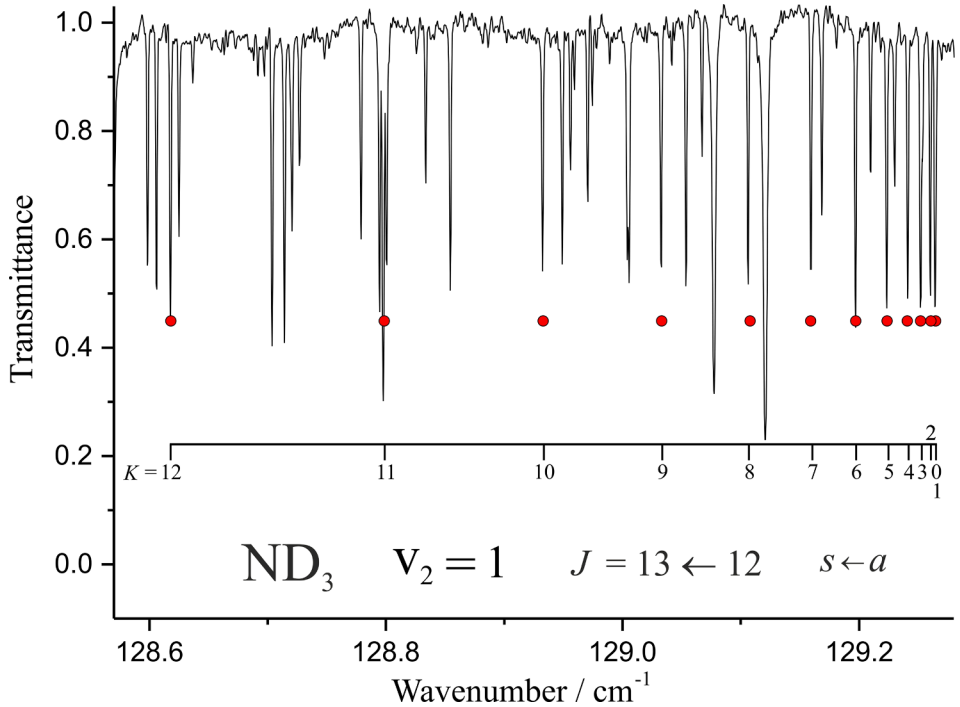

Fig. 3. Portion of the rotation-inversion spectrum for ND_3 in the $v_2 = 1$ state showing the $s \leftarrow a$ $R_K(12)$ transitions. Experiment: see the recording conditions of spectrum 3 in Table 1.

4. Analyses, results and discussion

4.1. Ground state analysis and results

The former experimental database [20] has been enlarged adding 510 rotation-inversion transitions and 1052 GSCD from transitions in ν_2, ν_4 and $2\nu_2$. The data have been analyzed adopting the methodology used in [20] and the reduced rotation-inversion Hamiltonian for the GS of ammonia [30] [and references therein]. The term values of the rotation-inversion levels were obtained as eigenvalues of the appropriate energy matrices. The diagonal elements were calculated from the following expression, which includes terms up to the 10th power in the angular momentum:

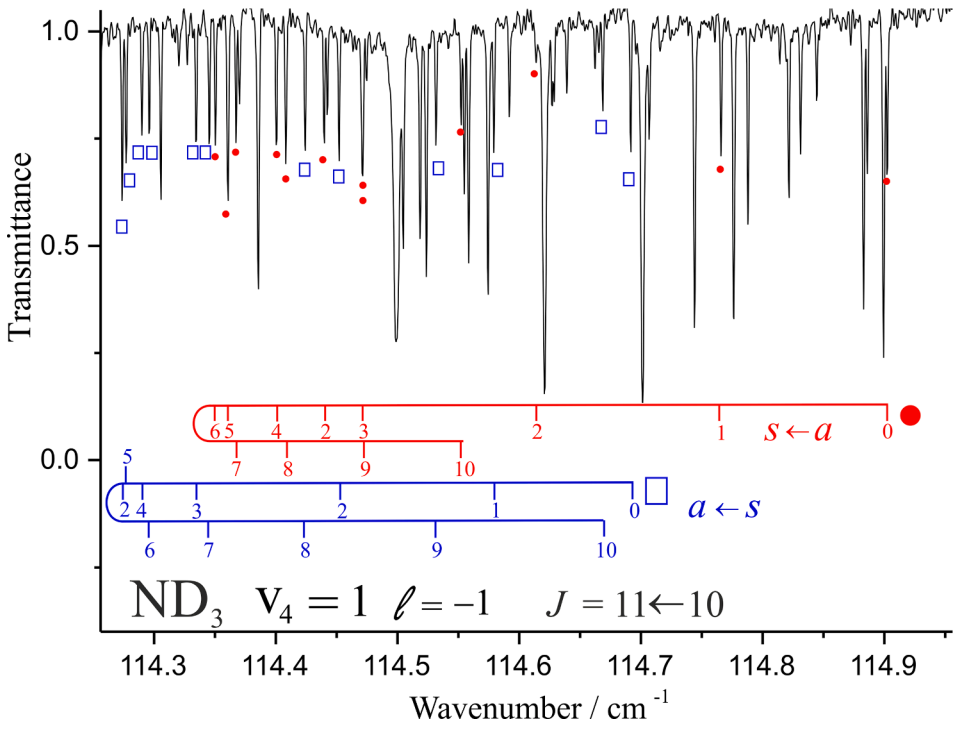

Fig. 4. Portion of the rotation-inversion spectrum for ND_3 in the $v_4 = 1$, $l = -1$ state showing the $s \leftarrow a$ and $a \leftarrow s$ $R_K(10)$ transitions. Experiment: see the recording conditions of spectrum 3 in Table 1.

$$
\begin{aligned}
{}^{(i)}E_v(J,k)/hc = {}&{}^{(i)}E_v^0 + {}^{(i)}B_v\left[J(J+1)-k^2\right] + {}^{(i)}C_v k^2 - {}^{(i)}D_{vJ}[J(J+1)]^2 - {}^{(i)}D_{vJK}[J(J+1)]k^2 - {}^{(i)}D_{vK}k^4 + \\
&+ {}^{(i)}H_{vJ}[J(J+1)]^3 + {}^{(i)}H_{vJJK}[J(J+1)]^2k^2 + {}^{(i)}H_{vJKK}[J(J+1)]k^4 + {}^{(i)}H_{vK}k^6 + \\
&+ {}^{(i)}L_{vJ}[J(J+1)]^4 + {}^{(i)}L_{vJJJK}[J(J+1)]^3k^2 + {}^{(i)}L_{vJJKK}[J(J+1)]^2k^4 + {}^{(i)}L_{vJKKK}[J(J+1)]k^6 + \\
&+ {}^{(i)}L_{vK}k^8 + {}^{(i)}M_{vJ}[J(J+1)]^5 + {}^{(i)}M_{vJJJJK}[J(J+1)]^4k^2 + {}^{(i)}M_{vJJJKK}[J(J+1)]^3k^4 + \\
&+ {}^{(i)}M_{vJJKKK}[J(J+1)]^2k^6 + {}^{(i)}M_{vJKKKK}[J(J+1)]k^8 + {}^{(i)}M_{vK}k^{10}
\end{aligned}
\tag{1}
$$

where (i) corresponds to (s) and (a) for the lower and upper components of the inversion doublets, representing the parity of the level with respect to the inversion; $k = \pm K$; v = 0 for GS.

The off-diagonal elements for the $\Delta k = \pm 3$ and $\Delta k = \pm 6$ interactions are given by

$$
\begin{aligned}
{}^{s}_{a}\langle \nu_s, J, k|(H_{04}+H_{06}+H_{08})/hc\,|\nu_s, J, k\pm 3\rangle^{a}_{s} = {}&\{[\alpha + \alpha_J J(J+1) + \alpha_{JJ}J^2(J+1)^2](2k\pm 3) + \\
&+[\alpha_K + \alpha_{JK}J(J+1)][k^3 + (k\pm 3)^3] + \alpha_{KK}[k^5 + (k\pm 3)^5]\}F_{\pm 3}(J,k)
\end{aligned}
\tag{2}
$$

$$
{}^{s}_{a}\langle \nu_s, J, k|(H_{06}+H_{08})/hc\,|\nu_s, J, k\pm 6\rangle^{s}_{a} = \left\{ {}^{(i)}\eta_3 + {}^{(i)}\eta_{3J}J(J+1) + {}^{(i)}\eta_{3K}\left[k^2 + (k\pm 6)^2\right] \right\}F_{\pm 6}(J,k) \tag{3}
$$

where

$$
F_{\pm n}(J,k) = [J(J+1) - k(k\pm 1)]^{1/2}[J(J+1) - (k\pm 1)(k\pm 2)]^{1/2}\ldots\{J(J+1) - [k\pm(n-1)](k\pm n)\}^{1/2}
$$

As usual, in the least squares analysis a statistical weight proportional to the inverse of its squared estimated uncertainty is assigned to each datum. The database contains 4744 data from the literature: 78 MW inversion transitions [26], 6 rotation-inversion transitions

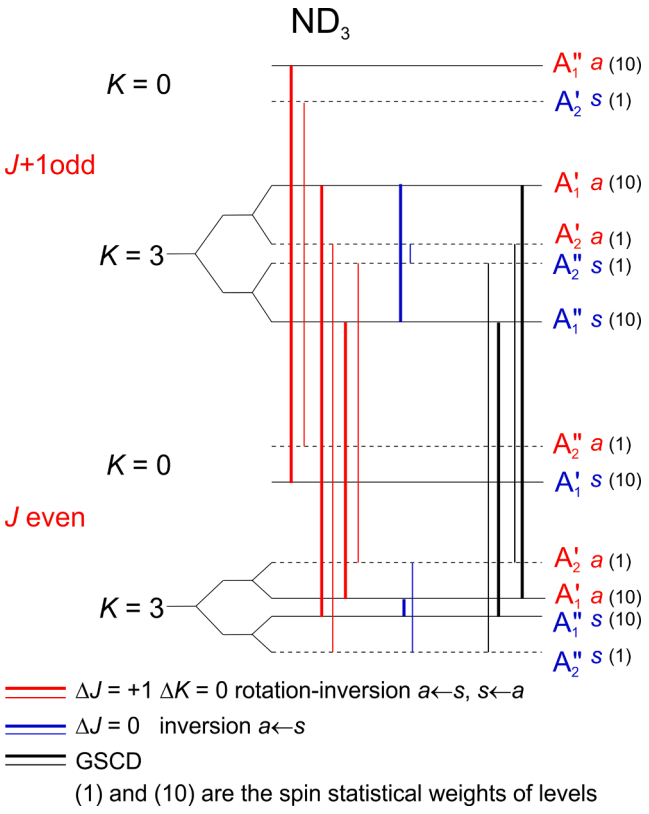

Fig. 5. Energy diagram showing the inversion-rotation levels for $K = 0$ and $K = 3$ in the GS of $^{14}ND_3$. Values in parentheses are the spin statistical weights of levels and those with the lower statistical weight are indicated by dashed lines. Observed inversion and rotation-inversion transitions are indicated by blue and red arrows, respectively. The ground state combination differences are indicated by black arrows. Thin and thick lines refer to weak and strong transitions, respectively. The splittings are enhanced for clarity. (For interpretation of the references to colour in this figure legend, the reader is referred to the web version of this article.)

measured in the sub-mmW region [27,28], 15 FIR rotation-inversion transitions [29], and 4645 GSCD calculated from 3522 IR transitions in $\nu_1/2\nu_4/\nu_3$ [17,20]. According to the literature an uncertainty of 0.01 or 0.02 MHz was attributed to the MW data, 0.1, 0.2 or 0.25 MHz to the sub-mmW transitions, 0.25×10^{-3} cm^{-1} to the unblended FIR transitions from [29], and 1.0×10^{-3} cm^{-1} to wavenumbers of ν_1, $2\nu_4$ and ν_3 isolated transitions [17,20]. The newly assigned data, 816 rotation-inversion and 4020 vibration-rotation-inversion transitions in $\nu_2/2\nu_2/\nu_4$ have uncertainty 0.1×10^{-3} and 0.4×10^{-3} cm^{-1}, respectively. Moreover, in case of unresolved $K = 3$ doublets an uncertainty of 0.1×10^{-2} cm^{-1} was given to the FIR transition connecting levels with lower statistical weight. The GSCD uncertainty is derived from the corresponding uncertainties σ_i and σ_j of ν_i and ν_j as $\sqrt{\left(\sigma_i^2 + \sigma_j^2\right)}$. Finally, in order to take into account the redundancy of the obtained GSCD each weight was multiplied by a factor equal to $(n\text{-}1/N)$, where n is the number of transitions sharing a common upper level, and N is the number of possible GSCD derived thereof.

In the iterative fitting procedure a rejection limit is used, which is gradually decreased from one iteration to the next and finally set to three times the estimated experimental uncertainties. In the last cycle of refinement, the transition wavenumbers whose observed minus calculated values exceed the rejection limit are excluded from the fit. After each iteration, the statistical significance of the obtained parameters is checked as well as their correlation coefficients. Several fits have been performed refining different sets of diagonal parameters, in particular the $^{(i)}L$ and $^{(i)}M$ constants, and of the interaction coefficients α and η in Eqs. (2) and (3), in order to compare the fit quality, the statistical significance of the determined parameters and the correlations between them.

In the final cycle of the refining procedure 1161 data, 23 FIR and 1138 GSCD, mostly from $\nu_1/\nu_3/2\nu_4$ transitions [17,20], not satisfying the adopted rejection limit, have been discarded. The results of this optimal fit from 8095 data retained in the last cycle of iteration are collected in Table 4. All parameters of the model, listed in Eqs. (1)-(3) and not present in Table 4, were tentatively allowed to vary in the fitting procedures and were constrained to zero because they resulted statistically

Table 3
Experimental transitions and ground state combination differences (GSCD) for the ground state analysis of $^{14}ND_3$.

Data	selection rules	no. of data	J'_{max}	K'_{max}
MW inversion transitions	$\Delta J = 0, \Delta K = 0, a \leftarrow s$	78 [a]	19	18
sub-mmW rotation-inversion transitions	$\Delta J = 1, \Delta K = 0, a \leftarrow s$ / $s \leftarrow a$	6 [b] (3/3)	2/2	1/1
FIR rotation-inversion transitions	$\Delta J = 1, \Delta K = 0, a \leftarrow s$ / $s \leftarrow a$	791 (397/394)	31/31	30/30
FIR rotation-inversion transitions	$\Delta J = 1, \Delta K = 0, a \leftarrow s$ / $s \leftarrow a$	15[c] (8/7)	5/5	4/4
FIR rotation-inversion transitions	$\Delta J = 1, \Delta K = \pm 3, s \leftarrow s$ / $a \leftarrow a$	25 (8/17)	12/12	6/8
GSCD from $\nu_2/2\nu_2/\nu_4$	$\Delta J = 1{,}2, \Delta K = 0$ / $\Delta K = \pm 3$	3696 (3058/638)	24/16	22/12
GSCD from $\nu_1/2\nu_4/\nu_3$	$\Delta J = 1{,}2, \Delta K = 0$ / $\Delta K = \pm 3$	4645 [d] (2219/2426)	19/13	18/13

[a] Ref.[26].
[b] Refs.[27,28].
[c] Ref.[29].
[d] Ref. [20].

Table 2
Transitions included in the current dataset the of $v_2 = 1$, 2 and $v_4 = 1$ *a*, *s* states of $^{14}ND_3$.

Band	Type of transitions	Selection rules		No. of lines	Observed J'_{max}	Observed K'_{max}
$\nu_2 \leftarrow \nu_2$	MW inversion	$\Delta J = 0, \Delta k = 0$	$a \leftarrow s$	78 [a]	16	13
$\nu_2 \leftarrow \nu_2$	FIR rotation-inversion	$\Delta J = +1, \Delta k = 0$	$a \leftarrow s$, $s \leftarrow a$	258/241	23/23	21/21
$2\nu_2 \leftarrow 2\nu_2$	FIR inversion	$\Delta J = 0, \Delta k = 0$	$a \leftarrow s$	72	16	16
$2\nu_2 \leftarrow 2\nu_2$	FIR rotation-inversion	$\Delta J = \pm 1, \Delta k = 0$	$a \leftarrow s$	153	17	16
$\nu_4 \leftarrow \nu_4$	FIR rotation-inversion	$\Delta J = +1, \Delta l = 0, \Delta k = 0$	$a \leftarrow s$, $s \leftarrow a$	283/272	18/19	17/17
$2\nu_2 \leftarrow \nu_2$	IR vibration-rotation-inversion	$\Delta J = 0, \pm 1, \Delta k = 0$	$a \leftarrow s$, $s \leftarrow a$	456/450	19/19	18/19
$\nu_4 \leftarrow \nu_2$	IR vibration-rotation-inversion	$\Delta J = 0, \pm 1, \Delta(k - l) = 0$	$s \leftarrow s$, $a \leftarrow a$	469/549	17/17	16/17
$2\nu_2 \leftarrow \nu_4$	FIR vibration-rotation-inversion	$\Delta J = 0, \pm 1, \Delta(k - l) = 0$	$s \leftarrow s$, $a \leftarrow a$	225/239	12/11	10/10
$\nu_2 \leftarrow GS$	IR vibration-rotation-inversion	$\Delta J = 0, \pm 1, \Delta k = 0$	$a \leftarrow s$, $s \leftarrow a$	782/761	23/23	22/23
$\nu_2 \leftarrow GS$	IR vibration-rotation-inversion	$\Delta J = 0, \pm 1, \Delta k = \pm 3$	$s \leftarrow s$, $a \leftarrow a$	43/34	12/12	12/7
$\nu_4 \leftarrow GS$	IR vibration-rotation-inversion	$\Delta J = 0, \pm 1, \Delta(k - l) = 0$	$s \leftarrow s$, $a \leftarrow a$	896/894	21/21	21/21
$\nu_4 \leftarrow GS$	IR vibration-rotation-inversion	$\Delta J = 0, \pm 1, \Delta(k - l) = \pm 3$	$a \leftarrow s$, $s \leftarrow a$	69/90	15/15	10/9
$2\nu_2 \leftarrow GS$	IR vibration-rotation-inversion	$\Delta J = 0, \pm 1, \Delta k = 0$	$a \leftarrow s$, $s \leftarrow a$	183/268	16/18	16/18

[a] from Ref. [25].

Table 4
Ground state spectroscopic parameters (in cm^{-1}) of $^{14}ND_3$

Parameter		*s*		*a*	
$^{(i)}E^0$ [b]		0.0 [c]		0.05308907255	(15211)
$^{(i)}B$		5.14275369725	(54409)	5.14257993618	(54416)
$^{(i)}C$		3.1381426141	(22246)	3.13823053490	(22246)
$^{(i)}D_J$	$\times 10^3$	0.1971894609	(47864)	0.1968867002	(47779)
$^{(i)}D_{JK}$	$\times 10^3$	–0.349572769	(12478)	–0.348678176	(12451)
$^{(i)}D_K$	$\times 10^3$	0.312932220	(38984)	0.312274917	(38982)
$^{(i)}H_J$	$\times 10^6$	0.023188720	(18051)	0.022818020	(17877)
$^{(i)}H_{JJK}$	$\times 10^6$	–0.075448937	(57081)	–0.073847460	(56337)
$^{(i)}H_{JKK}$	$\times 10^6$	0.085957053	(70896)	0.083661731	(70095)
$^{(i)}H_K$	$\times 10^6$	0.89891174	(22432)	0.90000908	(22429)
$^{(i)}L_J$	$\times 10^9$	–0.004249824	(25645)	–0.003935302	(24756)
$^{(i)}L_{JJJK}$	$\times 10^9$	0.015267978	(67134)	0.013484109	(60923)
$^{(i)}L_{JJKK}$	$\times 10^9$	–0.014309414	(77177)	–0.010403150	(75681)
$^{(i)}L_{JKKK}$	$\times 10^9$	0.0 [c]		–0.003880902	(42869)
$^{(i)}L_K$	$\times 10^9$	0.0 [c]		0.001446889	(16349)
$^{(i)}M_J$	$\times 10^{12}$	0.000720551	(12426)	0.000590954	(11197)
$^{(i)}M_{JJJJK}$	$\times 10^{12}$	–0.000839633	(30427)	0.0 [c]	
$^{(i)}M_{JJJKK}$	$\times 10^{12}$	0.002134717	(64865)	0.0 [c]	
$^{(i)}M_{JJKKK}$	$\times 10^{12}$	–0.02656843	(18139)	–0.02416694	(16636)
$^{(i)}M_{JKKKK}$	$\times 10^{12}$	0.04651551	(27504)	0.04553874	(27288)
$^{(i)}M_K$	$\times 10^{12}$	0.0 [c]		0.0 [c]	
Interaction parameters					
α	$\times 10^3$	0.037424777	(12774)		
α_J	$\times 10^6$	–0.00979261	(10175)		
α_K	$\times 10^6$	0.03252645	(12087)		
α_{JJ}	$\times 10^9$	0.00146173	(12829)		
α_{JK}	$\times 10^9$	–0.01942046	(17957)		
α_{KK}	$\times 10^9$	–0.04847731	(15818)		
Total number of fitted / assigned data 8095 / 9256	RMS				
No. of fitted / assigned MW data 78 / 78	0.0114 MHz				
No. of fitted / assigned FIR data 814 / 837	0.210×10^{-3} cm^{-1}				
No. of fitted / calculated GSCD from $\nu_2/2\nu_2/\nu_4$ 3595 / 3696	0.804×10^{-3} cm^{-1}				
No. of fitted / calculated GSCD from $\nu_1/2\nu_4/\nu_3$ 3608 /4645	2.207×10^{-3} cm^{-1}				

[a]The uncertainties as 1σ given in parentheses refer to the last significant digits and are reported with 5 digits to avoid round off errors in the calculation of the MW transitions.Identical energy levels are obtained by simultaneously reversing the sign of all the $\Delta k = \pm 3$ interaction constants α's.
[b] $^{(a)}E^0$ is the inversion splitting in the ground state for $J = K = 0$.
[c] Constrained.

undetermined or did not improve the quality of the fit.

All parameters are statistically well determined, most of them with high precision. Their uncertainties are reported with 5 least significant digits to avoid round off errors in the reproduction of the MW transitions from [26]. The set of parameters in Table 4 can be compared to those listed in Table 2 of Ref. [20]. The 10th order $^{(i)}M$ centrifugal parameters and the α_{JJ}, α_{JK}, and α_{KK} coefficients have been refined, thanks to the higher J and K values of the FIR transitions in the new database. The values of corresponding parameters are very similar, the percentage differences being about zero with the exception of the $^{(i)}L$, α_J and α_K, whose differences range from 10% to 40%. However, due to the higher precision of the experimental data, the parameters in Table 4 have smaller uncertainties. The root mean squared (RMS) errors of MW, FIR and GSCD data listed in Table 4 are in good agreement with the experimental uncertainties estimated for the different types of data. As expected, the RMS value for the GSCD from transitions in $\nu_2/2\nu_2/\nu_4$ decreases from 1.145×10^{-3} cm^{-1} in [20] to 0.804×10^{-3} cm^{-1}.

The transition frequencies or wavenumbers, assignments and residuals calculated using the parameters in Table 4 are listed in Table S1 in order of increasing values of J'' and K''. The rotational symmetry of the lower state of transition in case of $K'' = 3$ can be derived from Fig. 5 taking into account that $K'' = -3$ in Table S1 is the level with lower energy in the doublet. The term values of *s* and *a* rotational levels in the GS calculated using the parameters in Table 4 are listed in Table S2. The computer code and the input data files are available from the authors upon request [31].

4.2. Theoretical model for the excited vibration states

The implemented theoretical Hamiltonian model adopted for $^{15}NH_3$ [21] is applied to $^{14}ND_3$. The relative position of the $v_2 = 1$, $v_4 = 1$ and $v_2 = 2$ states in $^{14}ND_3$ illustrated in Fig. 1 suggests that the interactions in the $\nu_2/\nu_4/2\nu_2$ bending system is of global nature as discussed in [17]. The ro-vibration analysis has been performed simultaneously on six states, the *s* and *a* components of $v_2 = 1$, 2 and $v_4 = 1$, taking into account explicitly all symmetry allowed interactions between and within them [21]. For each value of J the program builds four Hamiltonian matrices. Two of them, with $k = 3p$ ($p = 0, \pm1, \pm2,\ldots$), are set up for levels of symmetry A' and A'' and contain eigenvalues of A_1', A_2' and A_1'', A_2'' rotational species. The other two correspond to one of the two (degenerate) blocks of E' and E'' symmetry. The blocks are numerically diagonalized to obtain the energy levels. The diagonal matrix elements, containing the usual contributions up to the 10th power in the angular momentum operators, are given by

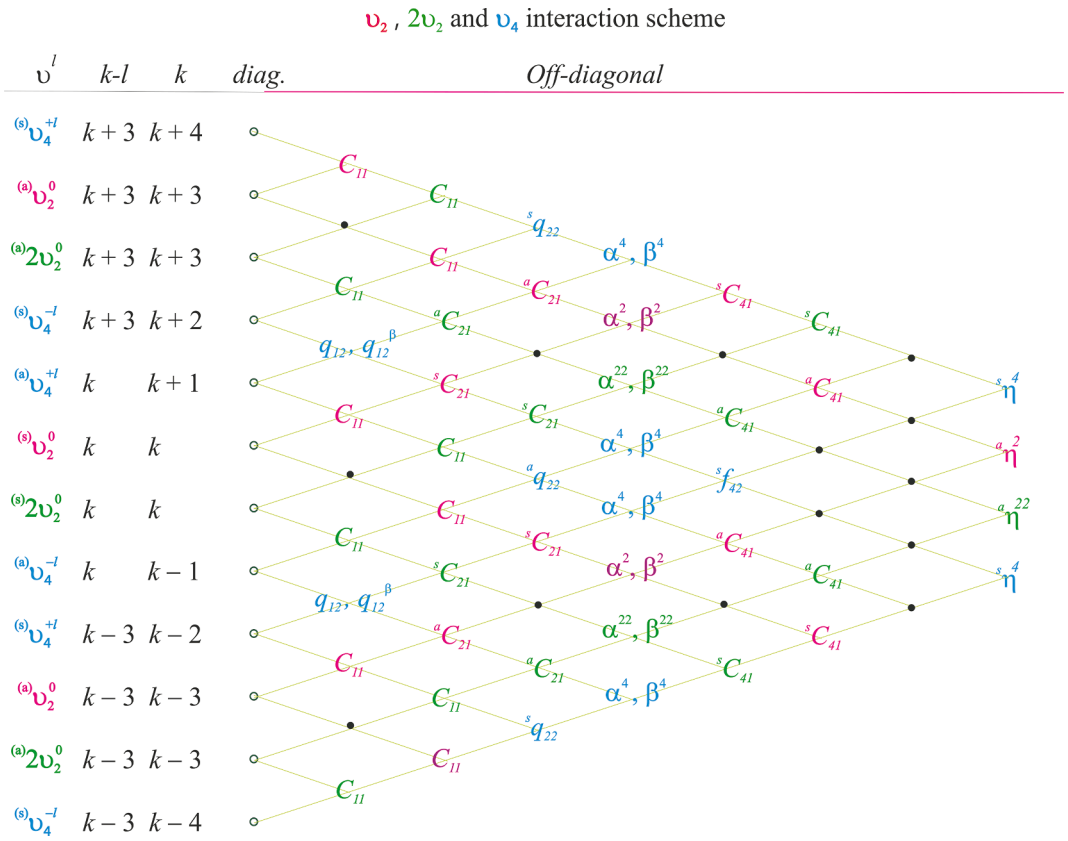

Fig. 6. Scheme of interactions in the energy matrix of the $\nu_2/\nu_4/2\nu_2$ system. For clarity, only the leading parameter of the off-diagonal matrix elements reported in Appendix A is shown. An identical scheme is obtained exchanging the *a*, *s* inversion symmetry of the interacting levels.

$$
\begin{aligned}
{}^{(i)}E_{\mathrm{v}}(J,k,l)/hc = {}&{}^{(i)}E_{\mathrm{v}}^{0} + {}^{(i)}B_{\mathrm{v}}\left[J(J+1)-k^2\right] + {}^{(i)}C_{\mathrm{v}}k^2 - 2\,{}^{(i)}(C\zeta)_{\mathrm{v}}kl - {}^{(i)}D_{\mathrm{v}J}[J(J+1)]^2 \\
&- {}^{(i)}D_{\mathrm{v}JK}[J(J+1)]k^2 - {}^{(i)}D_{\mathrm{v}K}k^4 + {}^{(i)}\eta_{\mathrm{v}J}[J(J+1)]kl + {}^{(i)}\eta_{\mathrm{v}K}k^3l \\
&+ {}^{(i)}H_{\mathrm{v}J}[J(J+1)]^3 + {}^{(i)}H_{\mathrm{v}JJK}[J(J+1)]^2k^2 + {}^{(i)}H_{\mathrm{v}JKK}[J(J+1)]k^4 \\
&+ {}^{(i)}H_{\mathrm{v}K}k^6 + {}^{(i)}L_{\mathrm{v}J}[J(J+1)]^4 + {}^{(i)}L_{\mathrm{v}JJJK}[J(J+1)]^3k^2 + {}^{(i)}L_{\mathrm{v}JJKK}[J(J+1)]^2k^4 \\
&+ {}^{(i)}L_{\mathrm{v}JKKK}[J(J+1)]k^6 + {}^{(i)}L_{\mathrm{v}K}k^8 \\
&+ {}^{(i)}\tau_{\mathrm{v}J}[J(J+1)]^2kl + {}^{(i)}\tau_{\mathrm{v}JK}[J(J+1)]k^3l + {}^{(i)}\tau_{\mathrm{v}K}k^5l + {}^{(i)}\tau^{*}_{\mathrm{v}K}k^3l^3 \\
&+ {}^{(i)}M_{\mathrm{v}J}[J(J+1)]^5 + {}^{(i)}M_{\mathrm{v}JJJK}[J(J+1)]^4k^2 + {}^{(i)}M_{\mathrm{v}JJKK}[J(J+1)]^3k^4 \\
&+ {}^{(i)}M_{\mathrm{v}JJKKK}[J(J+1)]^2k^6 + {}^{(i)}M_{\mathrm{v}JKKKK}[J(J+1)]k^8 + {}^{(i)}M_{\mathrm{v}K}k^{10}
\end{aligned}
\tag{4}
$$

where (*i*) refers to the parity of the level with respect to the inversion, *s* or *a*; $k = \pm K$; v = $v_2 = 1$, $v_2 = 2$, or $v_4 = 1$; $l = l_4 = \pm 1$. All terms containing *l* vanish for the $v_2 = 1$, 2 states.

The off-diagonal matrix elements are reported in Appendix A, where H_{mn} represents a group of terms in the Hamiltonian containing *m* vibrational operators q_r and/or p_r, and *n* rotational operators J_α [32]. The subscript of the interaction constants in the Appendix A represents the Δk and Δl selection rules for the levels connected by the interaction term in the Hamiltonian. Moreover, an interaction constant without the left superscript (*i*) corresponds to an $s \leftrightarrow a$ resonance, while an (*s*) or (*a*) superscript represents interaction between levels of the same parity where there is no ambiguity, i.e. ${}^{(s)}q_{22}$, ${}^{(s)}q^{J}_{22}$, ${}^{(s)}q^{K}_{22}$, ${}^{(s)}f_{42}$, ${}^{(s)}f^{J}_{42}$, ${}^{(s)}f^{K}_{42}$, ${}^{(s)}C^{2}_{21}$, etc.. For the Coriolis coefficients, ${}^{(i)}C^{1}_{11}$, ${}^{(i)}C^{2}_{11}$, ${}^{(i)}C^{3a}_{11}$ and ${}^{(i)}C^{3b}_{11}$, the superscript (*i*) refers to the parity of the interacting $v_2 = 1$ or $v_2 = 2$ level. The (*s*) and (*a*) interaction parameters can be refined independently. In case of the Coriolis type resonances, the coefficients of the H_{31}, H_{32}, H_{33} and H_{34} Hamiltonian terms that connect $v_2 = 2$ and $v_4 = 1^{\pm 1}$ are written with the same symbols used for the coefficients of H_{21}, H_{22}, H_{23} and H_{24}, that connect $v_2 = 1$ and $v_4 = 1^{\pm 1}$. This choice is consistent with the observation that in both cases the levels interact according to the same Δk and Δl selection rules. The interaction scheme for the $\nu_2/2\nu_2/\nu_4$ band system is illustrated in Fig. 6 where, for clarity, only the leading parameter of each off-diagonal matrix element is reported. The computer code and the input data files are available to researchers from the authors upon requests [31].

4.3. Analysis of the excited vibrational states and results

The 7765 experimental data from Table 2 have been fitted to the parameters of Eq. (4) and to those reported in Appendix A. The GS term values used to calculate the transition wavenumbers of the cold bands were obtained as eigenvalues from the appropriate energy matrices, using the GS parameters of Table 4. The statistical weight assigned to

Table 5
Spectroscopic parameters (in cm^{-1}) of the $v_2 = 1$, 2 and $v_4 = 1$ *a*, *s* excited vibration states of $^{14}ND_3$[a]

Parameter	$v_2 = 1$ *s*	$v_2 = 1$ *a*	$v_2 = 2$ *s*	$v_2 = 2$ *a*	$v_4 = 1^{\pm 1}$ *s*	$v_4 = 1^{\pm 1}$ *a*
E^0	745.59742429(4211)	749.14502424(4210)	1359.04937219(6513)	1430.05035034(6758)	1190.50259659(5342)	1190.57171367(5388)
B	5.226705562(1182)	5.216791970(1179)	5.239203828(3876)	5.095379443(3647)	5.174968085(2306)	5.174715015(2249)
C	3.103427962(1686)	3.108666279(1685)	3.010992756(3651)	3.082321385(3793)	3.117345066(2322)	3.117467080(2393)
$D_J \times 10^3$	0.23048216(1457)	0.21807982(1489)	0.27350784(6323)	0.15082494(5356)	0.20851940(2951)	0.20792096(2841)
$D_{JK} \times 10^3$	–0.40662282(2501)	–0.36707979(2441)	–0.5890093(1387)	–0.24045992(1213)	–0.39175853(6237)	–0.38881488(5918)
$D_K \times 10^3$	0.34066511(1915)	0.31017541(1865)	0.48903640(9172)	0.24472833(8311)	0.32965096(4277)	0.32726872(4194)
$H_J \times 10^6$	0.03324143(2978)	0.02139527(2824)	0.0224859(3906)	–0.0157159(3031)	0.0295864(1509)	0.0265910(1444)
$H_{JJK} \times 10^6$	–0.09977348(9526)	–0.04721489(7880)	–0.070195(1261)	0.0641674(9944)	–0.1113603(5003)	–0.0946172(4676)
$H_{JKK} \times 10^6$	0.1154381(1675)	0.0374944(1456)	0.050090(1497)	–0.088264(1185)	0.1376398(5973)	0.1128279(5655)
$H_K \times 10^6$	0.8761437(1025)	0.91447449(9454)	0.9300629(6598)	0.9700324(5500)	0.8754610(2579)	0.8872431(2618)
$L_J \times 10^9$	–0.00757606(3145)	–0.00130381(2789)	0.0236195(7990)	0.0128313(5667)	–0.0083954(2636)	–0.0017347(2466)
$L_{JJJK} \times 10^9$	0.03834585(8154)	0.0 [b]	–0.154946(3491)	–0.056888(2473)	0.049801(1088)	0.0104628(9978)
$L_{JJKK} \times 10^9$	–0.0858527(2093)	0.00053079(9516)	0.376069(6334)	0.098395(4308)	–0.090008(1602)	–0.023953(1489)
$L_{JKKK} \times 10^9$	0.0847832(2234)	0.0 [b]	–0.345273(5389)	–0.081256(3461)	0.0564037(8065)	0.0200177(7955)
$L_K \times 10^9$	–0.0115621(1351)	0.01917325(8512)	0.117858(1839)	0.040073(1230)	0.0 [b]	0.0 [b]
$C\zeta$					–0.975805981(3967)	–0.976001545(4067)
$\eta_J \times 10^3$					0.3202017(1112)	0.3192545(1161)
$\tau_{JK} \times 10^6$					0.084620(2980)	0.093046(3014)
$\tau_K \times 10^6$					–5.687144(2988)	–5.692186(3052)

Interaction parameters

ν_2/ν_4				$2\nu_2/\nu_4$	
$^{(s)}C^1_{11}$	3.4087[b]	$^{(a)}C^{3a}_{11} \times 10^3$	–0.4289228(1474)	$^{(s)}C^1_{11}$	0.29466467(9043)
$^{(a)}C^1_{11}$	3.4036[b]	$^{(s)}C^2_{11} \times 10^3$	–5.249[b]	$^{(a)}C^1_{11}$	0.2302988(1696)
$^{(s)}C^2_{21}$	0.018516297(9532)	$^{(a)}C^2_{11} \times 10^3$	–5.275[b]	$^{(s)}C^2_{21}$	–0.00579413(3041)
$^{(a)}C^2_{21}$	0.018513669(9576)	$^{(s)}C^3_{21} \times 10^3$	0.370678(1165)	$^{(a)}C^2_{21}$	–0.00578710(3784)
$^{(s)}C^{3a}_{11} \times 10^3$	–0.4146207(1371)	$^{(a)}C^3_{21} \times 10^3$	0.330083(1028)	$^{(s)}C^3_{21} \times 10^3$	–0.212979(1031)
				$^{(a)}C^3_{21} \times 10^3$	–0.163784(2884)

ν_2		$2\nu_2$		ν_4	
$\alpha^2 \times 10^3$	0.02426346(4028)	$\alpha^{22} \times 10^3$	0.02317237(2929)	$\alpha^4 \times 10^3$	0.0481908(1489)
$\alpha^2_J \times 10^6$	–0.0090254(1362)	$\alpha^{22}_J \times 10^6$	0.0050866(1216)	$q_{12} \times 10^3$	–8.594580(4340)
$\alpha^2_K \times 10^6$	0.0253874(2860)	$\alpha^{22}_K \times 10^6$	0.0 [b]	$f^K_{12} \times 10^6$	4.0143(1179)

Total number of fitted/assigned transitions 7630/7765
Standard deviation of an observation of unit weight 1.28

[a] The uncertainties as 1σ given in parentheses refer to the last significant digits and are reported with 4 digits to avoid round off errors in the calculation of the MW transitions.
[b] Constrained, see text.

each experimental datum in the global fit was proportional to the inverse of its squared estimated uncertainty. An uncertainty of 0.05 or 0.10 MHz was attributed to the MW transitions from [25], 0.2×10^{-3} cm^{-1} to the isolated inversion and rotation-inversion FIR transitions, and 0.4×10^{-3} cm^{-1} to the cold and hot band transitions. Moreover, the uncertainty of each assigned wavenumber was multiplied by the factor $\sqrt{n}$, with n being the number of overlapping transitions using the average of the corresponding calculated wavenumbers as calculated values.

Several fits were performed refining different sets of parameters. In each cycle of the fitting procedure the transition wavenumbers differing from their corresponding calculated values by more than a chosen rejection limit, which was gradually decreased from one iteration to the next, were excluded from the data set. After each iteration, the statistical significance of the obtained parameters was checked as well as their correlation coefficients. Very high correlations between many refined parameters were observed and, in order to reduce them, the Coriolis constants for the interaction between $v_2 = 1$ and $v_4 = 1$, $^{(s)}C^1_{11}$, $^{(a)}C^1_{11}$, $^{(s)}C^2_{11}$ and $^{(a)}C^2_{11}$ were fixed to the values obtained during the final iteration, 3.4087, 3.4036, -5.249×10^{-3} and -5.275×10^{-3} cm^{-1}, respectively. With a chosen limit of rejection of five times the experimental uncertainty, 135 of 7765 data, corresponding to 1.7 %, were excluded in the last cycle. About 20 % of the discarded transitions are randomly distributed being poorly measured or blended lines while the remaining ones correspond mainly to transitions with high J' and K' values.

The 118 refined spectroscopic parameters of the optimal fit are collected in Table 5. They comprise 6 vibration term values, 26, 28 and 34 diagonal parameters for the *s*, *a* levels in $v_2 = 1$, 2 and $v_4 = 1$. Ten interaction coefficients between ν_2/ν_4 and six between $2\nu_2/\nu_4$ have been refined. Moreover, six α coefficients of the $\Delta l = 0, \Delta k = \pm 3$ interaction and two coefficients of the essential resonances in $v_4 = 1$, q_{12} and f^K_{12}, have been determined. All spectroscopic parameters in Table 5 are statistically well determined and are at least three times larger than their uncertainties. Their uncertainties are reported with 4 least significant digits to avoid round off errors in the reproduction of the MW transitions from [25]. All parameters of the model, listed in Eq. (4) or in Appendix A, and not present in Table 5, were tentatively allowed to vary in the fitting procedures and were constrained to zero because they resulted statistically undetermined or did not improve the quality of the fit, i.e. number of fitted lines and standard deviation.

The internal consistency of the *s* and *a* corresponding parameters in the excited states is evaluated. The percentage differences of the *s* and *a* values for *B* and *C* amount to 0.2 % in $v_2 = 1$ and 2.0 % in $v_2 = 2$. The values for the *D*'s and for *H*'s are 7.5 % and 50 % on average in $v_2 = 1$ while in $v_2 = 2$ they increase to about 50 % and 150 %. The differences between corresponding *s* and *a* parameters are at least one order of magnitude larger than their counterparts in the GS. This partly reflects the number and strength of perturbations in the excited states with respect to the GS, and the increased inversion splittings. In $v_4 = 1$ the values of the *s* and *a* *B*, *C*, $C\zeta$, *D*'s, *H*'s, η's and τ's constants are very similar with percentage differences that vary from 0.01 to 18 %. Differences of about 70 % on average are seen for *L*'s, being their values more effective. Due to the more extended database with respect to [17], the *L* diagonal parameters for $v_2 = 2$ and $v_4 = 1$, and the interaction coefficients $^{(i)}C^2_{21}$ in ν_2/ν_4 and $2\nu_2/\nu_4$, $^{(i)}C^3_{21}$ in $2\nu_2/\nu_4$ and f^K_{12} in $v_4 = 1^{\pm 1}$

Table 6
Fit results for subset of transitions assigned to the $\nu_2/2\nu_2/\nu_4$ band system of $^{14}ND_3$.

Band		assigned / fitted transitions	J'_{max}	K'_{max}	RMS/10^{-3} cm^{-1}
ν_2	$a \leftarrow s$, $a \leftarrow a$	816 / 811	23	22	0.42
ν_2	$s \leftarrow a$, $s \leftarrow s$	804 / 790	23	23	0.42
$\nu_2 \leftarrow \nu_2$	$a \leftarrow s$	336 / 333	23	21	0.22
$\nu_2 \leftarrow \nu_2$	$s \leftarrow a$	241 / 241	23	21	0.26
ν_4^{-1}	$s \leftarrow s$, $s \leftarrow a$	472 / 450	20	20	0.56
ν_4^{-1}	$a \leftarrow a$, $a \leftarrow s$	460 / 436	20	20	0.48
ν_4^{+1}	$s \leftarrow s$, $s \leftarrow a$	514 / 506	21	21	0.51
ν_4^{+1}	$a \leftarrow a$, $a \leftarrow s$	503 / 499	21	21	0.57
$\nu_4^{-1} \leftarrow \nu_2$	$s \leftarrow s$	230 / 230	15	14	0.58
$\nu_4^{-1} \leftarrow \nu_2$	$a \leftarrow a$	280 / 280	15	15	0.53
$\nu_4^{+1} \leftarrow \nu_2$	$s \leftarrow s$	239 / 239	17	16	0.40
$\nu_4^{+1} \leftarrow \nu_2$	$a \leftarrow a$	269 / 269	17	17	0.44
$\nu_4^{-1} \leftarrow \nu_4^{-1}$	$s \leftarrow a$	132 / 132	18	16	0.43
$\nu_4^{-1} \leftarrow \nu_4^{-1}$	$a \leftarrow s$	145 / 141	18	17	0.39
$\nu_4^{+1} \leftarrow \nu_4^{+1}$	$s \leftarrow a$	140 / 136	19	17	0.37
$\nu_4^{+1} \leftarrow \nu_4^{+1}$	$a \leftarrow s$	138 / 136	18	16	0.39
$2\ \nu_2$	$a \leftarrow s$	183 / 183	16	16	0.66
$2\ \nu_2$	$s \leftarrow a$	268 / 262	18	18	0.59
$2\ \nu_2 \leftarrow \nu_2$	$a \leftarrow s$	456 / 454	19	18	0.40
$2\ \nu_2 \leftarrow \nu_2$	$s \leftarrow a$	450 / 424	19	19	0.47
$2\ \nu_2 \leftarrow 2\nu_2$	$a \leftarrow s$	225 / 214	17	16	0.32
$2\nu_2 \leftarrow \nu_4^{-1}$	$s \leftarrow s$	86 / 86	10	10	0.58
$2\nu_2 \leftarrow \nu_4^{-1}$	$a \leftarrow a$	101 / 101	10	10	0.59
$2\nu_2 \leftarrow \nu_4^{+1}$	$s \leftarrow s$	139 / 139	12	10	0.61
$2\nu_2 \leftarrow \nu_4^{+1}$	$a \leftarrow a$	138 / 138	11	10	0.62

have been refined. The values of the *s* and *a* diagonal parameters are very similar to the corresponding ones in [17] with the exception of $^{(i)}D_K$, $^{(i)}H_K$, and $^{(a)}L_K$ reflecting the new results of these constants in the GS. The *B*, *C*, *D*'s, *H*'s *a*, *s* parameters of $v_2 = 1$ and 2 are comparable to their corresponding ones in the GS. For both states the percentage differences amount to less than two units for *B* and *C*, to few tens for the *D*'s, and to few hundreds for the *H*'s parameters. The α coefficients in the GS and in $v_2 = 1$, 2 and $v_4 = 1$ have comparable values. An analogous significant comparison for α_J and α_K is prevented by the different number of the higher order coefficients refined, see Tables 4 and 5. It should be remembered that the order of the energies for the A_1', A_2' and A_1'', A_2'' levels for $K = 3, 6, \ldots$. depends on the relative signs of the *α's* constants. The values of the Coriolis coefficients $^{(i)}C_{11}^1$ and $^{(i)}C_{11}^2$ for the dyad ν_2/ν_4 are reported in Table 5 without uncertainties since they were kept fixed in the final cycle of the refinement, owing to a very strong correlation with $^{(i)}B_{v2=1}$, which prevented the parameters to be refined simultaneously. Thanks to this choice many parameters in the final fit resulted free from significant internal correlations but some strong correlations could not be avoided. They are present between $^{(s)}E^0_{v2=1}$ and $^{(a)}E^0_{v2=1}$, $^{(s)}B_{v2=1}$ and $^{(a)}B_{v2=1}$, $^{(s)}C_{v2=1}$ and $^{(a)}C_{v2=1}$, which are 100% correlated, while $^{(i)}\tau_{JK}$ with $^{(i)}\tau_K$ and $^{(s)}C^3_{21}$ with $^{(s)}C^2_{21}$ in $v_2 = 1$ are 99% correlated. Many attempts were done to lower those correlations, i.e. fixing the *s* and *a* interaction coefficients to the same value or changing the number and types of interactions constants. Since the set of interaction coefficients in Table 5 play a crucial role in the data reproduction we preferred to refine them, despite the presence of unavoidable high correlations. The standard deviation of an observation of unit weight, 1.28, is not far from 1, confirming that the uncertainties estimated for the experimental data are reliable and that the adopted model is adequate.

The RMS errors of the fit for different sets of experimental data are reported in Table 6. They compare very well with the uncertainties attributed to the data in the least squares procedure.

Finally, the values of the harmonic frequencies, the anharmonicity constants, and the vibration–rotation interaction constants α's for $^{14}ND_3$ that could be derived from the vibrational term values and the rotational constants in Tables 4 and 5 are listed in Table 7.

The transition frequencies or wavenumbers, assignments and residuals calculated using the parameters in Tables 4 and 5 are listed in Table S3 in order of increasing energy. In case of blended absorption lines the calculated values in column 11th are the average of their frequencies or wavenumbers while in column 15th the calculated values have not been averaged. The data set is divided into many portions in Table S4, grouping the transitions, listed in order of increasing J' and K' values, according to the upper and lower vibration states. Both Tables have been deposited to the Editor as Supplementary Materials.

Table 7
Harmonic wavenumbers, anharmonicity constants and vibration-rotation interaction constants (in cm^{-1}) of $^{14}ND_3$[a].

	s	*a*
$^{(i)}\omega_2^0$	811.6701(1)	783.2649(1)
$^{(i)}x_{22}$	–66.0727(1)	–34.1199(1)
$^{(i)}\alpha_2^B$	–0.083952(1)	–0.074212(1)
$^{(i)}\alpha_2^C$	0.034715(3)	0.029564(2)
$^{(i)}\alpha_4^B$	–0.032214(2)	–0.032135(2)
$^{(i)}\alpha_4^C$	0.020798(3)	0.020763(2)

[a] Term values of $v_2 = 1$, 2 *a*, *s* and $^{(i)}B_0$, $^{(i)}C_0$, $^{(i)}B_{v2=1}$, $^{(i)}C_{v2=1}$, $^{(i)}B_{v4=1}$, $^{(i)}C_{v4=1}$ values are from Tables 4 and 5.

5. Conclusions

Thanks to the high resolution spectra of $^{14}ND_3$ recorded in the region 60 – 1515 cm^{-1} using the facilities of the Synchrotron Canadian Light Source the spectroscopic analyses of the GS and of the $\nu_2/2\nu_2/\nu_4$ band system have been done at experimental accuracy. The assignments of the rotation-inversion transitions in the GS, $v_2 = 1$, 2 and $v_4 = 1$ and of the vibration-rotation-inversion transitions in the cold and hot bands have been implemented both in number and precision. The new databases have been analyzed together with all the data from the literature. In the analysis of the excited states the model adopted to reproduce 7765 data considers simultaneously the *a* and *s* components of $\nu_2/2\nu_2/\nu_4$ band system. The effective Hamiltonian used for the analysis includes all

symmetry allowed interactions between and within the studied excited state levels. 7630 experimental transitions retained in the final cycle of the least squares analysis resulted in the refinement of 118 spectroscopic parameters, all statistically well determined. They allow the calculation of precise values of the vibration-rotation-inversion levels of the excited states up to high J and K values. The analysis of the 9256 GS data comprising 8341 GSCD from the transitions in $\nu_2/2\nu_2/\nu_4$ and $\nu_1/2\nu_4/\nu_3$ systems, allowed the determination of an improved set of GS constants and the calculation of the energy term values up to $J/K = 31/30$. The present investigation improves the spectroscopic characterization of the GS and of the $v_2 = 1$, 2 and $v_4 = 1$ *a*, *s* states for $^{14}ND_3$ and enlarges its line lists. This can be useful for the observation of exoplanet atmospheres, planet-forming disk, cold stars, comets and interstellar medium investigated by the James Webb Space Telescope, whose MID-IR spectrograph covers the wavenumber range in the analysed spectra [33]. These results could also noticeably improve the wavenumber line list in the HITRAN and CDMS databases [23,34].

Credit authorship contribution statement

Elisabetta Canè: Conceptualization, Methodology, Formal analysis, Investigation, Resources, Data curation, Supervision, Validation, Writing – original draft, Writing – review & editing. **Gianfranco Di Lonardo:** Formal analysis, Investigation, Writing – review & editing. **Luciano Fusina:** Conceptualization, Methodology, Formal analysis, Investigation, Resources, Data curation, Software, Writing – original draft, Writing – review & editing. **Adriana Predoi-Cross:** Data acquisition, Writing – review & editing. **Filippo Tamassia:** Supervision, Project administration, Funding acquisition, Writing – review & editing.

Declaration of Competing Interest

The authors declare that they have no known competing financial interests or personal relationships that could have appeared to influence the work reported in this paper.

Data availability

Data will be made available on request.

Acknowledgements

EC and FT acknowledge the financial support from the Università di Bologna (RFO2021). We thank Dr. B. Billinghurst for recording the ammonia spectra at the Canadian Light Source, a national research facility of the University of Saskatchewan, which is supported by the Canada Foundation for Innovation (CFI), the Natural Sciences and Engineering Research Council (NSERC), the National Research Council (NRC), the Canadian Institutes of Health Research (CIHR), the Government of Saskatchewan, and the University of Saskatchewan.

Appendix A

Off–diagonal matrix elements of the vibration–rotation–inversion Hamiltonian[1] [a]

$$ {}^{s}_{a}|v_2 v_4^{l_4}, J, k\rangle = {}^{s}_{a}|10^0, J, k\rangle = {}^{s}_{a}|\nu_2, J, k\rangle; $$

The basis functions are $ {}^{s}_{a}|v_2 v_4^{l_4}, J, k\rangle = {}^{s}_{a}|01^{\pm 1}, J, k\rangle = {}^{s}_{a}|\nu_4^{\pm 1}, J, k\rangle; $

$$ {}^{s}_{a}|v_2 v_4^{l_4}, J, k\rangle = {}^{s}_{a}|20^0, J, k\rangle = {}^{s}_{a}|2\nu_2, J, k\rangle $$

Coriolis type resonances

$$ {}^{s}_{a}\langle \nu_2, J, k|(H_{21}+H_{23})/hc|\nu_4^{\pm 1}, J, k\pm 1\rangle^{a}_{s} = \pm\sqrt{2}\{ {}^{(i)}C^{1}_{11} + {}^{(i)}C^{3a}_{11}J(J+1) + {}^{(i)}C^{3b}_{11}[k^2+(k\pm 1)^2]\}F_{\pm 1} $$

$$ {}^{s}_{a}\langle \nu_2, J, k|(H_{22}+H_{24})/hc|\nu_4^{\pm 1}, J, k\pm 1\rangle^{a}_{s} = \sqrt{2}\{[{}^{(i)}C^{2}_{11} + {}^{(i)}C^{4a}_{11}J(J+1)](2k\pm 1) + {}^{(i)}C^{4b}_{11}[k^3+(k\pm 1)^3]\}F_{\pm 1} $$

$$ {}^{s}_{a}\langle \nu_2, J, k|(H_{22}+H_{24})/hc|\nu_4^{\mp 1}, J, k\pm 2\rangle^{s}_{a} = \sqrt{2}\{ {}^{(i)}C^{2}_{21} + {}^{(i)}C^{4a}_{21}J(J+1) + {}^{(i)}C^{4b}_{21}[k^2+(k\pm 2)^2]\}F_{\pm 2} $$

$$ {}^{s}_{a}\langle \nu_2, J, k|H_{23}/hc|\nu_4^{\mp 1}, J, k\pm 2\rangle^{s}_{a} = \pm\sqrt{2}\, {}^{(i)}C^{3}_{21}(2k\pm 2)F_{\pm 2} $$

$$ {}^{s}_{a}\langle \nu_2, J, k|H_{24}/hc|\nu_4^{\mp 1}, J, k\mp 4\rangle^{s}_{a} = \pm\{ {}^{(i)}C^{4}_{41} + {}^{(i)}C^{4a}_{41}J(J+1)\}F_{\pm 4} $$

$$ {}^{s}_{a}\langle 2\nu_2, J, k|(H_{31}+H_{33})/hc|\nu_4^{\pm 1}, J, k\pm 1\rangle^{a}_{s} = \pm\sqrt{2}\{ {}^{(i)}C^{1}_{11} + {}^{(i)}C^{3a}_{11}J(J+1) + {}^{(i)}C^{3b}_{11}[k^2+(k\pm 1)^2]\}F_{\pm 1} $$

$$ {}^{s}_{a}\langle 2\nu_2, J, k|(H_{32}+H_{34})/hc|\nu_4^{\pm 1}, J, k\pm 1\rangle^{a}_{s} = \sqrt{2}\{[{}^{(i)}C^{2}_{11} + {}^{(i)}C^{4a}_{11}J(J+1)](2k\pm 1) + {}^{(i)}C^{4b}_{11}[k^3+(k\pm 1)^3]\}F_{\pm 1} $$

$$ {}^{s}_{a}\langle 2\nu_2, J, k|(H_{32}+H_{34})/hc|\nu_4^{\mp 1}, J, k\pm 2\rangle^{s}_{a} = \sqrt{2}\{ {}^{(i)}C^{2}_{21} + {}^{(i)}C^{4a}_{21}J(J+1) + {}^{(i)}C^{4b}_{21}[k^2+(k\pm 2)^2]\}F_{\pm 2} $$

$$ {}^{s}_{a}\langle 2\nu_2, J, k|H_{33}/hc|\nu_4^{\mp 1}, J, k\pm 2\rangle^{s}_{a} = \pm\sqrt{2}\, {}^{(i)}C^{3}_{21}(2k\pm 2)F_{\pm 2} $$

$$ {}^{s}_{a}\langle 2\nu_2, J, k|H_{34}/hc|\nu_4^{\mp 1}, J, k\mp 4\rangle^{s}_{a} = \pm\{ {}^{(i)}C^{4}_{41} + {}^{(i)}C^{4a}_{41}J(J+1)\}F_{\pm 4} $$

$\Delta l = 0,\ \Delta k = \pm 3$ and $\Delta l = 0,\ \Delta k = \pm 6$ type resonances

[1] $F_{\pm n} = [J(J+1) - K(K\pm 1)]^{1/2}[J(J+1) - (K\pm 1)(K\pm 2)]^{1/2}.....\{J(J+1) - [K\pm(n-1)](K\pm n)\}^{1/2}$.

$$ {}^{s}_{a}\langle \nu_2, J, k|(H_{04}+H_{24}+H_{26})/hc|\nu_2, J, k\pm 3\rangle^{a}_{s}= \left\{ \begin{array}{c} \left[\alpha^2+\alpha_J^2 J(J+1)+\alpha_{JJ}^2 J^2(J+1)^2\right](2k\pm 3)+ \\ \left[\alpha_K^2+\alpha_{JK}^2 J(J+1)\right]\left[k^3+(k\pm 3)^3\right]+\alpha_{KK}^2\left[k^5+(k\pm 3)^5\right] \end{array} \right\} F_{\pm 3} $$

$$ {}^{s}_{a}\langle \nu_4^{\pm 1}, J, k|(H_{04}+H_{24}+H_{26})/hc|\nu_4^{\pm 1}, J, k\pm 3\rangle^{a}_{s}= \left\{ \begin{array}{c} \left[\alpha^4+\alpha_J^4 J(J+1)+\alpha_{JJ}^4 J^2(J+1)^2\right](2k\pm 3)+ \\ \left[\alpha_K^4+\alpha_{JK}^4 J(J+1)\right]\left[k^3+(k\pm 3)^3\right]+\alpha_{KK}^4\left[k^5+(k\pm 3)^5\right] \end{array} \right\} F_{\pm 3} $$

$$ {}^{s}_{a}\langle 2\nu_2, J, k|(H_{04}+H_{24}+H_{26})/hc|2\nu_2, J, k\pm 3\rangle^{a}_{s}= \left\{ \begin{array}{c} \left[\alpha^{22}+\alpha_J^{22} J(J+1)+\alpha_{JJ}^{22} J^2(J+1)^2\right](2k\pm 3)+ \\ \left[\alpha_K^{22}+\alpha_{JK}^{22} J(J+1)\right]\left[k^3+(k\pm 3)^3\right]+\alpha_{KK}^{22}\left[k^5+(k\pm 3)^5\right] \end{array} \right\} F_{\pm 3} $$

$$ {}^{s}_{a}\langle \nu_2, J, k|(H_{04}+H_{24}+H_{26})/hc|\nu_2, J, k\pm 3\rangle^{a}_{s}= -{}^{a}_{s}\langle \nu_2, J, k\pm 3|(H_{04}+H_{24}+H_{26})/hc|\nu_2, J, k\rangle^{s}_{a}= -\left\{\left[\beta^2+\beta_J^2 J(J+1)\right]+\beta_K^2\left[k^2+(k\pm 3)^2\right]\right\}F_{\pm 3} $$

$$ {}^{s}_{a}\langle \nu_4^{\pm 1}, J, k|(H_{04}+H_{24}+H_{26})/hc|\nu_4^{\pm 1}, J, k\pm 3\rangle^{a}_{s}= -{}^{a}_{s}\langle \nu_4^{\pm 1}, J, k\pm 3|(H_{04}+H_{24}+H_{26})/hc|\nu_4^{\pm 1}, J, k\rangle^{s}_{a}= -\left\{\left[\beta^4+\beta_J^4 J(J+1)\right]+\beta_K^4\left[k^2+(k\pm 3)^2\right]\right\}F_{\pm 3} $$

$$ {}^{s}_{a}\langle 2\nu_2, J, k|(H_{04}+H_{24}+H_{26})/hc|2\nu_2, J, k\pm 3\rangle^{a}_{s}= -{}^{a}_{s}\langle 2\nu_2, J, k\pm 3|(H_{04}+H_{24}+H_{26})/hc|2\nu_2, J, k\rangle^{s}_{a}= -\left\{\left[\beta^{22}+\beta_J^{22} J(J+1)\right]+\beta_K^{22}\left[k^2+(k\pm 3)^2\right]\right\}F_{\pm 3} $$

$$ {}^{s}_{a}\langle \nu_2, J, k|(H_{26}+H_{28})/hc|\nu_2, J, k\pm 6\rangle^{s}_{a}= \left\{ {}^{(i)}\eta_3^2+{}^{(i)}\eta_{3J}^2 J(J+1)+{}^{(i)}\eta_{3K}^2\left[k^2+(k\pm 6)^2\right]\right\}F_{\pm 6} $$

$$ {}^{s}_{a}\langle \nu_4^{\pm 1}, J, k|(H_{26}+H_{28})/hc|\nu_4^{\pm 1}, J, k\pm 6\rangle^{s}_{a}= \left\{ {}^{(i)}\eta_3^4+{}^{(i)}\eta_{3J}^4 J(J+1)+{}^{(i)}\eta_{3K}^4\left[k^2+(k\pm 6)^2\right]\right\}F_{\pm 6} $$

$$ {}^{s}_{a}\langle 2\nu_2, J, k|(H_{26}+H_{28})/hc|2\nu_2, J, k\pm 6\rangle^{s}_{a}= \left\{ {}^{(i)}\eta_3^{22}+{}^{(i)}\eta_{3J}^{22} J(J+1)+{}^{(i)}\eta_{3K}^{22}\left[k^2+(k\pm 6)^2\right]\right\}F_{\pm 6} $$

Essential resonances

$$ {}^{s}_{a}\langle \nu_4^{\mp 1}, J, k\pm 1|(H_{22}+H_{24})/hc\,|\nu_4^{\pm 1}, J, k\rangle^{a}_{s}= 2\left\{ \begin{array}{c} \left[q_{12}+f_{12}^{J} J(J+1)+f_{12}^{JJ} J^2(J+1)^2\right](2k\pm 1)+\left[f_{12}^{K}+f_{12}^{JK} J(J+1)\right] \\ \left[k^3+(k\pm 1)^3\right]+f_{12}^{KK}\left[k^5+(k\pm 1)^5\right] \end{array} \right\} F_{\pm 1} $$

$$ {}^{s}_{a}\langle \nu_4^{\mp 1}, J, k\pm 1|(H_{22}+H_{24})/hc\,|\nu_4^{\pm 1}, J, k\rangle^{a}_{s}= -2\left\{q_{12}^{\beta}+f_{12}^{\beta J} J(J+1)+f_{12}^{\beta K}(k^2+(k\pm 1)^2)\right\}F_{\pm 1} $$

$$ {}^{s}_{a}\langle \nu_4^{\mp 1}, J, k|(H_{22}+H_{24})/hc\,|\nu_4^{\pm 1}, J, k\pm 2\rangle^{s}_{a}= 2\left\{ \begin{array}{c} {}^{(i)}q_{22}+{}^{(i)}f_{22}^{J} J(J+1)+{}^{(i)}f_{22}^{JJ} J^2(J+1)^2+\left[{}^{(i)}f_{22}^{K}+{}^{(i)}f_{22}^{JK} J(J+1)\right] \\ \left[k^2+(k\pm 2)^2\right]+{}^{(i)}f_{22}^{KK}\left[k^4+(k\pm 2)^4\right] \end{array} \right\} F_{\pm 2} $$

$$ {}^{s}_{a}\langle \nu_4^{\mp 1}, J, k\pm 4|(H_{24}+H_{26})/hc\,|\nu_4^{\pm 1}, J, k\rangle^{s}_{a}= 2\left\{ \begin{array}{c} {}^{(i)}f_{42}+{}^{(i)}f_{42}^{J} J(J+1)+{}^{(i)}f_{42}^{JJ} J^2(J+1)^2+\left[{}^{(i)}f_{42}^{K}+{}^{(i)}f_{42}^{JK} J(J+1)\right] \\ \left[k^2+(k\pm 4)^2\right]+{}^{(i)}f_{42}^{KK}\left[k^4+(k\pm 4)^4\right] \end{array} \right\} F_{\pm 4} $$

the superscript (*i*) in the coefficients indicates the parity of the levels involved in the interaction and those of the $v_2 = 1, 2$ levels in case of ambiguity.

Appendix B. Supplementary data

Tables of the experimental and calculated wavenumbers for the transitions assigned in the ground state and in the $v_2 = 1$, 2 and $v_4 = 1$ *a*, *s* vibration states, and of term values for the ground state of $^{14}ND_3$ are given as S1 to S4. Supplementary data to this article can be found online at https://doi.org/10.1016/j.jms.2023.111797.

References

[1] X. Huang, K. Sung, G.C. Toon, D.W. Schwenke, A collaborative $^{14}NH_3$ IR spectroscopic analysis at 6000 cm^{-1}, J. Quant. Spectrosc. Radiat. Transf. 280 (2022), 108076, https://doi.org/10.1016/j.jqsrt.2022.108076.

[2] P. Cacciani, P. Čermák, J. Vander Auwera, A. Campargue, The ammonia absorption spectrum between 3900 and 4700 cm^{-1}. J. Quant. Spectrosc. Radiat. Transfer, 277 (2022) 107961, Doi: 10.1016/j.jqsrt.2021.107961.

[3] P. Čermák, P. Cacciani, J. Cosléou, Accurate The $^{14}NH_3$ line-list for the 2.3 μm spectral region. J. Quant. Spectrosc. Radiat. Transfer, 274 (2021) 107861, Doi: 10.1016/j.jqsrt.2021.107861.

[4] N.F. Zobov, T. Bertin, J. Vander Auwera, S. Civiš, A. Knížek, M. Ferus, R.I. Ovsyannikov, V.Yu. Makhnev, J. Tennyson, O.L. Polyansky, The spectrum of ammonia near 0.793 μm. J. Quant. Spectrosc. Radiat. Transfer, 273 (2021) 107838, Doi: 10.1016/j.jqsrt.2021.107838.

[5] J.W. Erisman, J.N. Galloway, S. Seitzinger, A. Bleeker, N.B. Dise, A.M. Roxana Petrescu, A.M. Leach, W. de Vries, Consequences of human modification of the global nitrogen cycle, Phil. Trans. R. Soc. B 368 (2013), https://doi.org/10.1098/rstb.2013.0116.

[6] S.J. Bolton, S.M. Levin, T. Guillot, C. Li, Y. Kaspi, G. Orton, M.H. Wong, F. Oyafuso, M. Allison, J. Arballo, S. Atreya, H.N. Becker, J. Bloxham, S.T. Brown, L. N. Fletcher, E. Galanti, S. Gulkis, M. Janssen, A. Ingersoll, J.L. Lunine, S. Misra, P. Steffes, D. Stevenson, J.H. Waite, R.K. Yadav, Z. Zhang, Microwave observations reveal the deep extent and structure of Jupiter's atmospheric vortices, Science 374 (2021) 968–972. https://science.org/doi/10.1126/science.abf1015.

[7] J. Huang, S. Seager, J.J. Petkowski, S. Ranjan, Z. Zhan, Assessment of Ammonia as a Biosignature Gas in Exoplanet Atmospheres, Astrobiology 22 (2022) 171–191, https://doi.org/10.1089/ast.2020.2358.

[8] J.E. Pineda, J. Harju, P. Caselli, O. Sipilä, M. Juvela, C. Vastel, E. Rosolowsky, A. Burkert, R.K. Friesen, Y. Shirley, M.J. Maureira, S. Choudhury, D.M. Segura-Cox, R. Güsten, A. Punanova, L. Bizzocchi, A.A. Goodman, An Interferometric View of H-MM1. I. Direct Observation of NH_3 Depletion, Astron. J. 163 (2022) 294, https://doi.org/10.3847/1538-3881/ac6be7.

[9] J.B. Bergner, Y.L. Shirley, J.K. Jørgensen, B. McGuire, S. Aalto, C.M. Anderson, G. Chin, M. Gerin, P. Hartogh, D. Kim, D. Leisawitz, J. Najita, K.R. Schwarz, A.G.G. M. Tielens, C.K. Walker, D.J. Wilner, E.J. Wollack, Astrochemistry With the Orbiting Astronomical Satellite for Investigating Stellar Systems, Front. Astron. Space Sci. 8 (2022), 793922, https://doi.org/10.3389/fspas.2021.793922.

[10] F.F.S. van der Tak, P. Schilke, H.S.P. Müller, D.C. Lis, T.G. Phillips, M. Gerin, E. Roueff, Triply deuterated ammonia in NGC 1333, A & A 388 (2002) L53–L56, https://doi.org/10.1051/0004-6361:20020647.

[11] D.C. Lis, E. Roueff, M. Gerin, T.G. Phillips, L.H. Coudert, F.F.S. van der Tak, P. Schilke, Detection of triply deuterated ammonia in the Barnard 1 cloud, Astrophys J 571 (2002) L55–L58, https://doi.org/10.1086/341132.

[12] E. Roueff, D.C. Lis, F.F.S. van der Tak, M. Gerin, P.F. Goldsmith, Interstellar deuterated ammonia: from NH_3 to ND_3, A & A 438 (2005) 585–598, https://doi.org/10.1051/0004-6361:20052724.

[13] D.C. Lis, M. Gerin, E. Roueff, T.G. Phillips, D.R. Poelman Interstellar deuteroammonia., Tracing physical conditions in dense, cold interstellar medium, Astrophys. Space Sci. 313 (2008) 77–80, https://doi.org/10.1007/s10509-007-9595-4.

[14] H. Roberts, E. Herbst, T.J. Millar, The chemistry of multiply deuterated species in cold, dense interstellar medium, A & A 424 (2004) 905–917, https://doi.org/10.1051/0004-6361:2004441.
[15] C. Ceccarelli, P. Caselli, D. Bockelée-Morvan, O. Mousis, S. Pizzarello, F. Robert, D. Semenov, Deuterium Fractionation: the Ariadne's Thread from the Pre-collapse Phase to Meteorites and Comets today, Protostars Planets V I (2014) 859–882.
[16] J. Harju, F. Daniel, O. Sipilä, P. Caselli, J.E. Pineda, R.K. Friesen, A. Punanova, R. Güsten, L. Wiesenfeld, P.C. Myers, A. Faure, P. Hily-Blant, C. Rist, E. Rosolowsky, S. Schlemmer, Y.L. Shirley, Deuteration of ammonia in the starless core Ophiuchus/H-MM1, A & A 600 (2017) A61, https://doi.org/10.1051/0004-6361/2016628463.
[17] E. Canè, G. Di Lonardo, L. Fusina, F. Tamassia, M. Villa, Infrared spectroscopy of $^{14}ND_3$: analysis of the $\nu_2/\nu_4/2\nu_2$ and $\nu_1/\nu_3/2\nu_4$ band systems, J. Quant. Spectrosc. Radiat. Transf. 203 (2017) 398–409, https://doi.org/10.1016/j.jqsrt.2017.03.028.
[18] L. Fusina, G. Di Lonardo, J.W.C. Johns, The ν_2 and ν_4 bands of $^{14}ND_3$, J. Mol. Spectrosc. 118 (1986) 397–423, https://doi.org/10.1016/0022-2852(86)90178.
[19] M. Snels, L. Fusina, H. Hollenstein, M. Quack, The ν_1 and ν_3 bands of ND_3, Mol. Phys. 98 (2000) 837–854, https://doi.org/10.1080/00268970050025457.
[20] L. Fusina, E. Canè, G. Di Lonardo, F. Tamassia, Perturbation allowed transitions in the infrared spectrum of $^{14}ND_3$: determination of the *K*-dependent parameters in the ground state, Mol. Phys. 116 (2018) 3538–3546, https://doi.org/10.1080/00268976.2018.1451003.
[21] E. Canè, G. Di Lonardo, L. Fusina, F. Tamassia, A. Predoi-Cross, The $v_2 = 1$, 2 and $v_4 = 1$ bending states of $^{15}NH_3$ and their analysis at experimental accuracy, J. Chem. Phys. 150 (2019), 194301, https://doi.org/10.1063/1.5088751.
[22] A.R.W. McKellar, High-resolution infrared spectroscopy with synchrotron sources, J. Mol. Spectrosc. 262 (2010) 1–10, https://doi.org/10.1016/j.jms.2010.04.006.
[23] I.E. Gordon, L.S. Rothman, R.J. Hargreaves, R. Hashemi, E.V. Karlovets, F.M. Skinner, E.K. Conway, C. Hill, R.V. Kochanov, Y. Tan, P. Wcisło, A.A. Finenko, K. Nelson, P.F. Bernath, M. Birk, V. Boudon, A. Campargue, K.V. Chance, A. Coustenis, B.J. Drouin, J.-M. Flaud, R.R. Gamache, J.T. Hodges, D. Jacquemart, E. J. Mlawer, A.V. Nikitin, V.I. Perevalov, M. Rotger, J. Tennyson, G.C. Toon, H. Tran, V.G. Tyuterev, E.M. Adkins, A. Baker, A. Barbe, E. Canè, A.G. Császár, A. Dudaryonok, O. Egorov, A.J. Fleisher, H. Fleurbaey, A. Foltynowicz, T. Furtenbacher, J.J. Harrison, J.-M. Hartmann, V.-M. Horneman, X. Huang, T. Karman, J. Karns, S. Kassi, I. Kleiner, V. Kofman, F. Kwabia-Tchana, N.N. Lavrentieva, T.J. Lee, D.A. Long, A.A. Lukashevskaya, O.M. Lyulin, V.Yu. Makhnev, W. Matt, S.T. Massie, M. Melosso, S.N. Mikhailenko, D. Mondelain, H.S.P. Müller, O.V. Naumenko, A. Perrin, O.L. Polyansky, E. Raddaoui, P.L. Raston, Z.D. Reed, M. Rey, C. Richard, R. Tóbiás, I. Sadiek, D.W. Schwenke, E. Starikova, K. Sung, F. Tamassia, S.A. Tashkun, J. Vander Auwera, I.A. Vasilenko, A.A. Vigasin, G.L. Villanueva, B. Vispoel, G. Wagner, A. Yachmenev, S.N. Yurchenko, The HITRAN2020 molecular spectroscopic database, J. Quant. Spectrosc. Radiat. Transfer, 277 (2022) 107949, Doi: 10.1016/j.jqsrt.2021.107949.
[24] E. Canè, G. Di Lonardo, L. Fusina, F. Tamassia, A. Predoi-Cross, Mono- and di-deuterated ammonias: far-infrared spectra and spectroscopic parameters in the ground state, J. Mol. Spectrosc. 384 (2022), 111581, https://doi.org/10.1016/j.jms.2022.111581.
[25] Š. Urban, D. Papousek, M. Bester, K. Yamada, G. Winniwisser, G. Guarnieri, Simultaneous analysis of the microwave and infrared spectra of 14ND3 and 15ND3 for the v2 excited state, J. Mol. Spectrosc. 106 (1984) 29–37, https://doi.org/10.1016/0022-2852(84)90080-8.
[26] L. Fusina, S.N. Murzin, Inversion Spectrum and Ground State Spectroscopic Parameters of $^{14}ND_3$, J. Mol. Spectrosc. 167 (1994) 464–467, https://doi.org/10.1006/jmsp.1994.1250.
[27] P. Helminger, W. Gordy, Sub-millimeter Wave Spectra of Ammonia and Phosphine, Phys. Rev. 188 (1969) 100–108, https://doi.org/10.1103/PhysRev.188.100.
[28] P. Helminger, F. De Lucia, W. Gordy, Rotational spectra of NH_3 and ND_3 in the 0.5-mm wavelength region, J. Mol. Spectrosc. 39 (1971) 94–97, https://doi.org/10.1016/0022-2852(71)90280-3.
[29] L. Fusina, G. Di Lonardo, J.W.C. Johns, Inversion-rotation spectrum and spectroscopic parameters of $^{14}ND_3$ in the ground state, J. Mol. Spectrosc. 112 (1985) 211–221, https://doi.org/10.1016/0022-2852(85)90205-X.
[30] K. Sarka, H.W. Schrötter, Effective Hamiltonian for rotation-inversion states of ammonia-like molecules, J. Mol. Spectrosc. 179 (1996) 195–204, https://doi.org/10.1006/jmsp.1996.0197.
[31] For academic uses only see the link https://www.unibo.it/sitoweb/elisabetta.cane/contenuti-utili.
[32] M.R. Aliev, J.K.G. Watson, Calculated sextic centrifugal distortion constants of polyatomic molecules, J. Mol. Spectrosc. 61 (1976) 29–52, https://doi.org/10.1016/0022-2852(76)90379-9.
[33] G.H. Rieke, G.S. Wright, T. Böker, J. Bouwman, L. Colina, A. Glasse, K.D. Gordon, T.P. Greene, M. Güdel, T.h. Henning, K. Justtanont, P.-O. Lagage, M.E. Meixner, H.-U. Nørgaard-Nielsen, T.P. Ray, M.E. Ressler, E.F. van Dishoeck, C. Waelkens, The Mid-Infrared Instrument for the James Webb Space Telescope, I: Introduction, Astronomical Society of the Pacific 127 (2015) 584–594, https://doi.org/10.1086/682252.
[34] H.S.P. Müller, S. Thorwirth, D.A. Roth, G. Winnewisser, The Cologne Database for Molecular Spectroscopy, CDMS, Astron Astrophys 370 (2001) L49–L52, https://doi.org/10.1051/0004-6361:20010367, https://cdms.astro.uni-koeln.de/.